Multiple geophysical surveys for old landfill monitoring in Singapore

Ke Yin[a,*], Huanhuan Tong[b], Apostolos Giannis[a], Jing-Yuan Wang[b], Victor W.-C. Chang[a,b]

[a]Residues and Resource Reclamation Centre (R3C), Nanyang Environment and Water Research Institute, Nanyang Technological University, 1 Cleantech Loop, CleanTech One, Singapore 637141, Singapore

[b]School of Civil and Environmental Engineering, Nanyang Technological University, 50 Nanyang Avenue, Singapore 639798, Singapore

Abstract

One-dimensional boring presents limitations on mapping the refuse profile in old landfills owning to waste heterogeneity. Electrical imaging (EI) and multiple-analysis of surface wave (MASW) was hereby deployed at an old dumping ground in Singapore to explore the subsurface in relation to geotechnical analysis. MASW estimated the refuse boundary with a higher precision as compared to EI, due to its endurance for moisture variation. EI and MASW transection profiles suggested spots of interest, e.g. refuse pockets and leachate mounds. 3D inversion of EI and MASW data further illustrated the transformation dynamics derived by natural attenuation, for instance the preferential infiltration pathway. Comparison of geophysical surveys at different years uncovered the subterranean landfill conditions, indicating strong impacts induced by ageing, precipitation and settlement. This study may shed light on a characterization framework of old landfills via combined geophysical models, thriving landfill knowledge with a higher creditability.

Keywords: geophysical method; EI; MASW; geotechnical analysis; landfill monitoring

* Corresponding author: yinke@ntu.edu.sg; Tel: +65 67904100

1. Introduction

Old landfills receive increasing attention due to their long-term environmental impacts, such as landfill gas emission and leachate outbreak. On top of that, urbanization has led to growing demands on land space. As such landfill redevelopment may alleviate the land scarcity meanwhile remove concerns. Therefore, a site characterization study is needed before taking action (Rattanaoudom 2005).

Usually, landfill characterization demands tremendous work that comprised of numerous boreholes and trial pits to obtain information of the subsurface in relation to its surrounding environment. The geotechnical works have little guidance in terms of borehole quality, quantity and location. Uncertainty or sometimes discrepancy may occur. Boring impediments, however, can be reduced with acquired knowledge of the subsurface. Herein geophysical approaches are scheduled. Combination of geotechnical and geophysical methods may provide better accuracy of landfill profile by leverage of respective advantage, i.e. specificity from boreholes and totality from geophysical methods. From the economic perspective, limited number of boreholes is translated into budget saving for geophysical survey and less destruction of the field (Dumont et al. 2016).

There is no single geophysical method that can fit all sites. Selection of geophysical methods depends on interpretation methodology and scope of work. In context of Lorong Halus Dumping Ground (LHDG), a technique capable of leachate detection is necessary at first. Secondly, the high precipitation in the tropics may request geophysical techniques with little influence by moisture. Also, the method should be commonly acceptable, affordable, and accessible.

Two specific geophysical methods are usually applied, electrical imaging (EI) and multiple-analysis of surface waves (MASW). EI measures the resistivity (or inversely, the

conductivity) contrasts between different materials. It has been applied in landfill characterization world widely (Kavazanjian et al. 1996; Svensson et al. 1999; Peace et al. 1996; NJDEP 2005; Grellier et al. 2007). EI can determine the main landfill characteristics e.g. the presence of percolated water, permeability of landfill liners, and dumping boundaries (Cardarelli and Di Filippo 2004). More specific properties such as the contaminated flow and groundwater movement direction was predicted in combination with topography and granite fracturing (Mota et al. 2004). Moreover, EI may be applied beyond post-closure stage covering stages during the planning, construction and operation (Reynolds and Taylor 1996). It is also deemed as the best choice in many identification work such as characterization of soil/unconsolidated layers, soil and rock properties, saltwater intrusion and soil salinity, etc. (ASTM 2011). MASW measures the contrast in seismic wave velocities as they move in between materials, thereby indicating the difference in stiffness of materials. In particular, surface wave (S-wave) method exhibits little influence by moisture while it has the uniquely reliable correlation to standard penetration test n (SPT-N) values, an important indicator for the soil strength. MASW has been successfully used for determining mechanical properties e.g. shear strength of the landfill body (Zekkos et al. 2014). But, it can aggressively characterize the landfill in terms of leachate- and gas/air- bearing zones and determine the density distribution of the subsurface (Konstantaki 2016).

As a result, EI and MASW were employed for geophysical mapping of LHDG.p3 in 2011 and 2013. The present study combined boring and geophysical analysis to develop an investigation framework for characterization of the old landfill from the perspective of natural attenuation.

2. Methodology

The Lorong Halus dumping ground phase 3 (LHDG.p3) was an uncontrolled dumping ground with little engineering works in application. It was originally a mangrove swamp

occupying about 44 ha. It was operated from 1983 to 1989 with the purpose of accepting MSW. However, in 1979 the completion of government incinerator resulted in gradual diversion of MSW into incineration ashes. Rapid urbanization in Singapore during 1980s generated huge amounts of construction and demolition (C&D) waste which had been landfilled as well. As a result, the buried wastes in LHDG.p3 were a mixture of MSW, incineration ashes and C&D waste (Montgomery Watson 1997). Since closure, no significant reclamation activities have been conducted except 2-5 m soil cover.

The site investigation comprised of two main thrusts: traditional geotechnical works and non-invasive geophysical surveys. Traditional investigations usually comprise of boring, sampling and a range of in-situ tests, and are also termed “invasive methods”. Boring activities produce borelogs that detail the subsurface profile within a specific confined location. Despite ground truth, the information is disconnected. Geophysical methods do not require penetration past the subsurface, working on the principles of measuring certain properties of a particular media and deducing the parameters of interest.

2.1. Soil Boring in 2013

Prior to drilling, cable detection work was carried out at all designated borehole locations. Trial pits up to at least 1.5 m depth were done at each borehole location to ascertain the absence of buried cables and services or any other man-made obstruction that could hinder drilling works. The technique employed was by rotary wash boring whereby boring was advanced by rotating drilling bit with cuttings removed by circulating water as the drilling fluid. Casings were used to support unstable grounds or when soft cohesive soil or non-cohesive soil was encountered during boring operations. The diameter of each drilled borehole was 100 mm. Soil sampling and loggings were done in accordance with BS5930 (the Code of Practice for Site Investigations, 1999). The land survey was conducted using a global positioning system/real time kinematic positioning (GPS/RTK) methodology. The

base station was set up at a known location and allowed RTK corrections to be transmitted in real time to the rover enable the high order accuracy of the survey coordinates and elevation to be determined. The indicative locations, elevation and termination depth of boring wells were accordingly recorded. Figure 1 presents the location of boring (BH1–5) and deployment details on geophysical investigation. Standard penetration test (SPT) was conducted in accordance with BS1377-9 (1990). The purpose of this empirical dynamic penetration test was to determine the dynamic shearing resistance of soils to the penetration of a split barrel sampler of 50 mm external diameter. It was driven by a 63.5 kg automatic drop hammer with a free fall height of 760 mm. The value of penetration resistance, "N" was the number of blows required to achieve a 300 mm penetration of the barrel. Number of blows required for every 150 mm penetration was recorded, normally only the last two records were used for N determination. SPT was conducted at specified depth when the subsoil was too stiff for undisturbed soil samples to be obtained. The values of N obtained in the investigation were recorded in bore logs. While the bore log was also recorded with continuous soil composition profiles particularly with information on refuse termination depth.

The collected samples were placed into laboratory-supplied wide-mouth glass containers and stored in an ice chest while on site and during transportation to an accredited geotechnical laboratory. Testing items were carried out including physical properties i.e. water content, bulk density, dry density and particle density, particle size distribution, Atterberg limits which were based on BS 1377 (1990), together with chemical properties including pH values (with a pH meter), organic matter (via TOC analyzer), sulfate (precipitation, separation followed by ignition) and chloride content (by titration with Volhard's method).

Fig. 1

2.2. Geophysical Surveys in 2011 & 2013

EI and MASW surveys were performed on an orthogonal test plot (100 m×100 m) orientated with existing gas extraction wells at each corner for spatial control (Fig. 1). Owning to a small scale investigation, the site ground was assumed as a geometric plane surface with the same elevation at 0 m. Each test comprised 24 survey lines subjected to both EI and MASW survey, among which 21 lines orientated parallel to the x-axis, positioned at 10 m intervals from 0 to 100 m southeast. In addition, 3 tie-lines orientated parallel to the y-axis. The tie-lines were included to restore linear features in the x-axis direction and to improve the data density (Bentley and Gharibi 2004; J. Chambers et al. 2002; J. E. Chambers et al. 2006).

2.2.1. EI method

EI was based on a current flow path between the current-potential electrodes. Dipole-dipole array configuration was adopted in the study as it was well suited to multi-channel systems (J. Chambers et al. 2002). The dipole-dipole array model was well received in geotechnical applications while especially in measuring lateral resistivity changes (Wightman et al. 2003). The field survey entailed the laying of metal rods (32) at 3 m interval on the ground, connected to cable then to multi-electrode resistivity meter together with a power booster. Manual measurement mode was applied, with a built-in 32 ch scanner and high power transmitter. Control system was equipped with CPU compatible to 586 and Interface named RS-232C. The EI survey included several steps. Firstly, vegetation was cleared with a width of around 2 m along the surveying line. A licensed surveyor was then marking the control points for the EI works, followed by setting of a series of potential dipoles which measured the resulting voltage gradient at each station along the line. Subsequent measurement was completed by moving the current dipole down the line. 10 m intervals were based on horizontal distance between two survey lines and the coordinates were accurately recorded. Forward earth modeling (2D) with finite-element method (FEM) inversion was

applied (ElecImager, Japan) to process raw data and generate the image (Coggon 1971; Pridmore et al. 1981; Holcombe and Jiracek 1984; Loke and Barker 1996). In brief, the apparent resistivity with depth was plotted and then contoured. EI was repeated in triplicates. The EI survey was employed twice at the same plot in the respective years of 2011 and 2013.

2.2.2. MASW method

MASW works based on properties that S-wave (mainly the Rayleigh wave) is equivalent to the shear waves (< 10% error) for earth materials with Poisson's ratios in the range of 0.25-0.48 while a depth less than 20-30 m (Wightman et al. 2003). MASW relies on frequency response and dispersion curves to obtain the subsurface profile. The seismic survey was measured with a seismic exploration system whereas the wave source was generated by hammering on a percussion plate. The system used for the study was a 24-channel seismograph with a natural frequency of geophones at 4.5 Hz, favoring landfill case. A total 24 geophones were fixed on the ground surface with the spike poked into the ground. Meanwhile two seismic land cables with twelve connectors were spread and connected with these geophones, through which electrical signal from each geophone was sent to the digital seismograph. A minimum of 12-geophone overlap condition was maintained for continuous adjacent spreads on the line. During field data acquisition, the operator adjusted the digital seismograph and confirmed the standby of the generating hammering source. After that, the operator monitored the noise condition on the display of the seismograph (for example, noise is caused by nodding of trees by wind and surface water). When it came to minimal noise condition, the operator instructed for hammering. To improve the resolution of near-surface interfaces, energy source positions were set at 1.5 m from the ends of the 3 m geophone spacing array. Multiple shots locations were utilized permitting interpretation of near-surface interfaces at various locations along the array and near the endpoints as well for variable subsurface profiles, and allowed more refined interpretations of shallow and mid-depth

subsurface velocities and interfaces. Shots were gathered to generate the dispersion curve in the frequency domain using the Common Mid Point (CMP) method. The inversion process was based on forward modeling to generate the 1D S-wave velocity distributions by software (SeisImager). For the comparison purpose, MASW surveys were employed twice at the same plot in the respective years of 2011 and 2013.

3. Results and Discussion

3.1. Bore logs

Five boreholes (BH1-5) were investigated with SPT-N values until depth of 30 m below ground level (BGL), with 20 measurements of each borehole (Fig. 1). Due to limited data points, Fig. 2 presents a collective result of the five boreholes. Hereby, geotechnical properties as a function of depth could be better elucidated. Interestingly, the collective data shows abnormal peaks at depth about 5-20 m BGL, where the values depart from a smooth rising trend and zoom steeply up to as high as 74. Except for the abruption, SPT-N values were well predicted with a gradual increase (Fig. 2a). The main purpose of the SPT-N test is to provide an indication of the relative density of granular deposits, such as sands and gravels from which it is virtually impossible to obtain undisturbed samples. However, the validity depends on the soil type. Analogously, the SPT-N values for the case of landfill do not necessarily depict the real in-situ physical properties. Instead, the sudden change of values may indicate a stratum compositionally distinct from its adjacent layers, supposing anthropogenic deposits. The large-size particles in the refuse layer may raise the SPT-N value due to clogging of the sampler or due to its contact with it (Machado et al. 2010). Soil sorting at the plot notes traceable amount of municipal solid wastes, such as plastics, woven fabrics and wood pieces at -8 to -15 m (Fig. S2), echoing the abrupt SPT-N elevation. Empirically S-

wave velocities may exhibit correlation with SPT-N values as investigated (Imai and Yoshimura 1982),

$V_s - 97.0N^{0.314}$ (Eq. 1)

Where the equation is valid when N stays in the range of 1–100, and V_s represents the S-wave velocity (m s^{-1}). Unfortunately the SPT-N values estimated by S-wave velocities (Fig. 2b) at BH5 displayed quite a difference from the real measurement particularly after depth -10 m albeit a good matching between L11 and L23, suggesting a poor correlation owning to the anthropogenic buries.

Fig. 2

SPT-Ns were compared between two depths i.e. -5–20 m vs. the rest (0 to -5 m and -20 to -30 m), suggesting statistically significantly difference between the two group of data with a p-value of 0.012. Comparisons were further made between R5 and R1–4 within each of the two depths (Fig. 2 c & 2d), showing poor linearity (R^2=0.25) in depth of -5–20 m too. It is very likely attributable for refuse deposits. As above, the refuse layer may be retrieved by SPT testing plot, from which abnormal SPT-N peaks are indicator for the refuse placement. Due to various compositions of wastes and complexity in the landfill, however, the subsurface stratum needs more data from other aspects for further characterization and identification.

Table 1

Further investigation of the landfill, such as water content, bulk and particle density, particle size distribution, organic matter, pH, sulfide and chloride concentration, and the Atterberg limit were carried out with regards to each borehole (Table 1). Saturated zone was not yet reached until the depth of -7 m as water content was measured less than void ratio. Interestingly, water content presented a positive correlation with void ratio (correl. coeff. =0.82) rather than depth (correl. coeff. =0.22), suggesting obstructed infiltration. As such

224 water may be isolated in pockets. The pockets may be developed by biogas, precipitation and
225 mineralization derived by natural attenuation. Geochemical measurements such as OM, pH,
226 sulfide and chloride show a characteristic of highly spot-specific, echoing the presence of
227 isolated pockets. Furthermore, particle size distribution posed much less influence on
228 moisture while it used to do. For example, a high silt/clay fraction 66% (w/w) was measured
229 at depth -4.5–5.3 m in BH3, however carrying a low water content (23%). Atterberg limit
230 tests showed a soil type with reduced plasticity (9–24), as a result from leachate permeation
231 (Frempong and Yanful 2008). The reduced plasticity of soil may facilitate the formation of
232 isolated pockets. Organic matter was measured low in the solid, indicating a late stage of the
233 landfill where most organic compounds had been stripped. The pH presented alkaline
234 suggesting a typical matured phase in the landfill as well. Low chloride was detected as well,
235 as a result of the long-term precipitation and dilution.

236 3.2. Refuse boundary

237 3.2.1. Estimation by borehole and geophysical methods

238 The refuse boundary was estimated with bore logs (Fig. 3). A contour map was
239 constructed by combining the refuse surface at different boreholes. Basically the refuse
240 boundary provided useful information to quantify the refuse volume, yet the leachate flow
241 direction was unlikely predicted without knowledge of the heterogeneous distribution of
242 density (Konstantaki 2016). The accuracy on refuse quantity could be compromised by the
243 limited boring number. Alternatively, the refuse layer could be indicated by geophysical
244 imaging (Soupios et al. 2007; Yin et al. 2015). Transection plots for S-wave velocity and
245 electrical resistivity are presented in Fig. 3 and Fig. 4 respectively, where the profiles at
246 survey Line 11 and Line 23 are displayed in combination with overlapped bore logs (BH1-
247 BH5-BH3 in Line 11 and BH4-BH5-BH2 in Line 23).

248 Fig. 3

Geotechnical parameters (BH1-5) and extracted geophysical data at the same sampling depths were statistically compared to obtain correlation coefficients (Table S1). Electrical resistivity carried a high correlation coefficient with chloride content (0.93)/moisture content (0.66). General poor correlations between S-wave velocity and soil properties though, bulk and dry density presented stronger correlations to S-wave velocity (0.36) than the others, indicating the dominance of hardness on S-wave propagation. Based on the analysis, there were existed significantly cohesive connections between geophysical data and the refuse characteristics, promising complementary explanation of the landfill subsurface. The refuse boundary could be estimated via the correspondent geophysical measures distinguishing the refuse layer from the original ground. The average depth of the refuse layer by MASW and EI at Line 11 was determined at -18.8±1.9 m and -18.0±4.2 m respectively, while 17.7±1.5 m and -24.2±4.7 m at Line 23. By contrast, bore logs showed a respective refuse depth of -18.6±1.0 m and -17.8±1.3 m. In this regards, MASW achieved a better compliance with bore logs, i.e. 18.8±1.9 m vs. 18.6±1.0 m BGL at Line 11 and 17.7±1.5 m vs. 17.8±1.3 m BGL at Line 23. Additional soil distribution beneath such as Kallang formation and old alluvium was indicated by MASW while not from EI (Balia and Littarru 2010). As moisture level highly affects electrical imaging, EI method may present a deteriorated depiction on the subsurface structure in tropics (Samouëlian et al. 2004; Brunet et al. 2010). Hence, edge effects may further compromise the results in EI tomography as shown in Fig. 5 (Griffiths and Lane 1999; Wu et al. 2013). Nonetheless, geophysical methods present improved details with the monitored parameter. In addition it may provide zones of interest carrying potential environmental significance.

Fig. 4 & 5

3.2.2. Comparison between EI and MASW

The S-wave velocity presented complex strata distribution across depth than electrical resistivity. Tomography of EI could be distinguished by three layers, a middle layer contained large areas of warm color (red and yellow) in pockets, in contrast to the more homogeneous upper and lower layer possessing mainly the cold colors (e.g. blue). The middle layer exhibited abrupt changes reference to its surroundings indicating the refuse distribution. The distinction suggests great variation on the corresponding material properties in middle layer, in association with water content, waste composition, physicochemical and biological activities, hydrogeology, etc. (Kibria and Hossain 2015). The upper and lower layer stands for a respective soil cover and the original surface, which could be easily identified by the consistent value strip of the resistivity together with a gentle rolling tomography.

Contrastively, MASW images showed more layers, suggesting more vertical changes of hardiness albeit the planar rolling (Hebeler 2001). It is relevant to the landfill design and operation as well as long-term natural attenuation, which amended the subsurface matrix e.g. the void ratio and density. The relative hard layer on top (0 to -4 m) indicated the soil cover. The strip next to it demonstrated interestingly minimum velocity, suggesting a porous zone with low density. With continuous natural attenuation, the organic matter was decomposed releasing biogas from bioactivity, resulting in reduced density and raised porosity. The high porosity up to 50% at 3–7 m BGL (Table 1) echoed such a hypothesis. The bulking property however, was less dominant in deeper layers, likely attributed to settlement and increased saturation (Das et al. 2002; Wall and Zeiss 1995). Moving deeper S-wave interfaces rolled severely. A couple reasons could be responsible for this. The original site of LHDG.p3 before landfilling was recorded as mangrove swamp carrying a soft nature (Yin et al. 2015). Besides, landfills often exhibit uneven settlement (Simões and Catapreta 2013; Chakma and Mathur 2012; Fei and Zekkos 2013). Deeper layers hereby bear these impacts and resulted in more

298 irregular distribution on the hardiness. In addition, infiltration could also pose an impact on
299 the harness distribution (Rosqvist and Destouni 2000).

300 3.3. 3D pseudo models

301 3D modeling of the landfill could provide further insights on waste transformation (Tame
302 et al. 2013). Figure 6 & 7 present pseudo-depth slices of EI and MASW simulating the plot
303 area in the years 2011 and 2013. An offset of 2.5 m was adopted to indicate changes of soil
304 profiles spanning a depth of 0–20 m. Comparisons were made based on (1) time, and (2)
305 contrasts of same spots.

306 Fig. 6 & 7

307 3.3.1. Landfill characterization by EI and MASW at different periods

308 Two scenarios were depicted in Fig. 6, dry scenario in 2011 and wet scenario in 2013.
309 The background electrical resistivity was recorded around 200±20 Ωm for both, indicating a
310 typical unsaturated zone with mixture of silt/sand in the subsurface (Fig. 6). Electrical
311 resistivity in 2013 were found from <100 to 500–600 Ωm, comparable to those observed
312 from two years ago. Interestingly, resistivity distribution across depth demonstrated an
313 opposite trend between two measurements, indicating a strong effect by the moisture
314 condition. The resistivity decreased with increased depth in 2013, suggesting a scenario under
315 infiltration. By contrast, growing resistivity along depth in 2011 suggested higher moisture at
316 the bottom—a stable state which occurred at the dry season. It evidenced that EI survey
317 compromised water content.

318 High uncertainty though from single EI investigation, hydrogeological conditions in the
319 subsurface could be indicated by comparison of the EI surveys at different periods (Sandberg
320 et al. 2002). For instance, preferential infiltration may occur at the middle of BH4 and BH5
321 from survey in 2013, while leachate mounding may exit below -15 m from survey in 2011
322 (Fig. 5). These findings provide advantages in further cares for the landfill if necessary.

323 Moreover, there existed some higher-resistivity pockets in 2013 as compared to 2011,
324 indicating the growing heterogeneity in the refuse due to natural attenuation.
325 Figure 7 shows comparison of S-wave velocity performed during the same periods as EI.
326 As compared to EI, MASW demonstrated little impacts from moisture changes (Fig. 7). The
327 background and trend of S-wave distribution was similar between 2011 and 2013.
328 Nevertheless, lower S-wave velocities was obtained at -5–10 m meanwhile higher in deeper
329 zones in 2013 as compared to 2011, which again suggests the geophysical changes in the
330 refuse layer towards more extremity. It may be developed from a few factors. On one hand
331 biochemical degradation facilitates settlement and leads to growing compaction at lower
332 layers reflected by a higher S-wave velocity. On the other hand the upper layer is subjected to
333 continuous loss of materials by leaching and dilution, thus a lower density—a lower S-wave
334 velocity.
335 3.3.2. Comparison of EI and MASW at different periods
336 As mentioned, EI is sensitive to environmental parameters relevant to conductivity,
337 including ionic strength and total dissolved solids etc., while MASW interests the
338 hardiness/stiffness of the zone, more relevant to settlement. Moisture effects on the EI
339 method have been well noted (Grellier et al. 2007; Bentley and Gharibi 2004). Also, moisture
340 is one of the significant factors posing long-term impacts on the refuse. In this point
341 comparison between the investigated geophysics could reveal extra information of the landfill
342 from perspectives e.g. the refuse components. Coupled with the findings from boring, more
343 refuse details may be unveiled from which a comprehensive diagnosis can be further
344 developed (Meju 2000). Taking account of time effect, transformation may be traceable.
345 At -2.5 m, all plots showed a stratum suggesting an artificial zone—the cover (Fig. 4). In
346 this layer the S-wave velocity measured low in both events while distinct resistivity was
347 identified between 2011 and 2013, indicating the presence of massive clay/silt which

possesses considerable water-holding capacity. At spots deeper below (e.g. -17.5–20 m in 2013) however, a high resistivity concurrent with a high S-wave velocity may indicate a zone of high porosity, where water is hardly retained. Soft zones at -5–10 m may be born from refuse deposit as shown in Fig. 7. Those red-color spots within the zones, which stand for low-moisture pockets (as shown in EI profile at -7.5–10 m in 2013 in Fig. 6), may fit to materials like plastics which carries both soft nature and hydrophobicity. Soil sorting study at the plot shows the affluence of plastics at -8-10 m, evidenced such a deduction (Fig. S3). Next to BH2–5 where dry spots were indicated by EI in 2013, it was peaked with S-wave velocity, suggesting a hard zone as well. The hardiness may be enforced by dryness which reduces the soil plasticity. The situation could be severer with time under limited water supply, unless precipitation promotes infiltration in the landfill and change the moisture content. As such geophysical methods may demonstrate the variation, identify anomalies and therefore provide effective while quantitative reading for the corresponding hot spots.

4. Conclusion

A geophysical modeling of an old landfill was developed with non-invasive geophysical methods. Cohesive correlations existed between geophysical data and geotechnical properties of boring samples. The subsurface profile can be well understood in combination of EI, MASW and limited boring. Transformation of the refuse layer may be predicted by integration of natural attenuation in landfills. Zones of interests could be determined with improved characteristic details such as soft material accumulation, isolated pocket, settling magnitude, moisture retention capacity and leachate mounding etc. Furthermore, long-term geophysical monitoring in the old landfill could indicate crucial parameters relevant to variation in environmental chemistry and hydrogeology of the landfill, assisted with a 3D

372 inversion. Preferential flow paths were herein well located to estimate the leachate
373 distribution.
374
375 Acknowledgements
376 This study is supported by the National Research Foundation of Singapore (NRF-CRP5-
377 2009-2), for Residues and Resource Reclamation Centre, Nanyang Technological University,
378 Singapore.

379 References

380 ASTM (2011). Standard guide for selecting surface geophysical methods. West
381 Conshohocken, PA: ASTM International.

382 Balia, R., & Littarru, B. (2010). Geophysical experiments for the pre-reclamation assessment
383 of industrial and municipal waste landfills. Journal of Geophysics and Engineering,
384 7(1), 64.

385 Bentley, L. R., & Gharibi, M. (2004). Two- and three-dimensional electrical resistivity
386 imaging at a heterogeneous remediation site. Geophysics, 69(3), 674-680,
387 doi:10.1190/1.1759453.

388 Brunet, P., Clément, R., & Bouvier, C. (2010). Monitoring soil water content and deficit
389 using Electrical Resistivity Tomography (ERT) – A case study in the Cevennes area,
390 France. Journal of Hydrology, 380(1–2), 146-153,
391 doi:http://dx.doi.org/10.1016/j.jhydrol.2009.10.032.

392 Cardarelli, E., & Di Filippo, G. (2004). Integrated geophysical surveys on waste dumps:
393 evaluation of physical parameters to characterize an urban waste dump (four case
394 studies in Italy). Waste Management & Research, 22(5), 390-402,
395 doi:10.1177/0734242x04046042.

396 Chakma, S., & Mathur, S. (2012). Estimation of Primary and Mechanical Compression in
397 MSW Landfills. Journal of Hazardous, Toxic, and Radioactive Waste, 16(4), 298-303,
398 doi:doi:10.1061/(ASCE)HZ.2153-5515.0000117.

399 Chambers, J., Ogilvy, R., Kuras, O., Cripps, J., & Meldrum, P. (2002). 3D electrical imaging
400 of known targets at a controlled environmental test site. Environmental Geology, 41(6),
401 690-704, doi:10.1007/s00254-001-0452-4.

402 Chambers, J. E., Kuras, O., Meldrum, P. I., Ogilvy, R. D., & Hollands, J. (2006). Electrical
403 resistivity tomography applied to geologic, hydrogeologic, and engineering

404 investigations at a former waste-disposal site. Geophysics, 71(6), B231-B239,
405 doi:doi:10.1190/1.2360184.
406 Coggon, J. H. (1971). Electromagnetic and electrical modeling by the finite element method.
407 Geophysics, 36(1), 132-155, doi:10.1190/1.1440151.
408 Das, K. C., Smith, M. C., Gattie, D. K., & Hale Boothe, D. D. (2002). Stability and quality of
409 municipal solid waste compost from a landfill aerobic bioreduction process. Advances
410 in Environmental Research, 6(4), 401-409, doi:http://dx.doi.org/10.1016/S1093-
411 0191(01)00066-1.
412 Dumont, G., Pilawski, T., Dzaomuho-Lenieregue, P., Hiligsmann, S., Delvigne, F., Thonart,
413 P., et al. (2016). Gravimetric water distribution assessment from geoelectrical methods
414 (ERT and EMI) in municipal solid waste landfill. Waste Management, 55, 129-140,
415 doi:http://dx.doi.org/10.1016/j.wasman.2016.02.013.
416 Fei, X., & Zekkos, D. (2013). Factors Influencing Long-Term Settlement of Municipal Solid
417 Waste in Laboratory Bioreactor Landfill Simulators. Journal of Hazardous, Toxic, and
418 Radioactive Waste, 17(4), 259-271, doi:doi:10.1061/(ASCE)HZ.2153-5515.0000167.
419 Frempong, E., & Yanful, E. (2008). Interactions between Three Tropical Soils and Municipal
420 Solid Waste Landfill Leachate. Journal of Geotechnical and Geoenvironmental
421 Engineering, 134(3), 379-396.
422 Grellier, S., Reddy, K., Gangathulasi, J., Adib, R., & Peters, C. (2007). Correlation Between
423 Electrical Resistivity and Moisture Content of Municipal Solid Waste in Bioreactor
424 Landfill. In Geoenvironmental Engineering (pp. 1-14).
425 Griffiths, D. V., & Lane, P. A. (1999). Slope stability analysis by finite elements.
426 Géotechnique, 49, 387-403

Hebeler, G. L. (2001). Site Characterization in Shelby County, Tennessee Using Advanced Surface Wave Methods: School of Civil and Environmental Engineering, Georgia Institute of Technology, 2001. Directed by Glenn J. Rix.

Holcombe, H. T., & Jiracek, G. R. (1984). Three-dimensional terrain corrections in resistivity surveys. Geophysics, 49(4), 439-452, doi:doi:10.1190/1.1441679.

Imai, T., & Yoshimura, Y. Correlation of N-value with S-wave velocity and shear modulus. In the 2nd European Symposium of Penetration Testing, Amsterdam, 1982 (pp. 57-72)

Kavazanjian, E., Matasovic, N., Stokoe, K. H., & Bray, J. D. In situ shear wave velocity of solid waste from surface wave measurements. In Second International Congress on Environmental Geotechnics, Osaka, Japan, 1996 (Vol. Proceedings 1, pp. 97-102)

Kibria, G., & Hossain, M. S. (2015). Investigation of degree of saturation in landfill liners using electrical resistivity imaging. Waste Management, 39(0), 197-204, doi:http://dx.doi.org/10.1016/j.wasman.2015.02.015.

Konstantaki, L. A. (2016). Imaging and characterization of heterogeneous landfills using geophysical methods.

Loke, M. H., & Barker, R. D. (1996). Practical techniques for 3D resistivity surveys and data inversion. Geophysical Prospecting, 44(3), 499-523.

Machado, S. L., Karimpour-Fard, M., Shariatmadari, N., Carvalho, M. F., & Nascimento, J. C. F. d. (2010). Evaluation of the geotechnical properties of MSW in two Brazilian landfills. Waste Management, 30(12), 2579-2591, doi:http://dx.doi.org/10.1016/j.wasman.2010.07.019.

Meju, M. A. (2000). Geoelectrical investigation of old/abandoned, covered landfill sites in urban areas: model development with a genetic diagnosis approach. Journal of Applied Geophysics, 44(2–3), 115-150, doi:http://dx.doi.org/10.1016/S0926-9851(00)00011-2.

451 Montgomery Watson (1997). Consultancy services for the rehabilitation of Tampines
452 dumping ground: site investigation and alternatives analysis. Final report (Vol. 1):
453 Montgomery Watson Pte Ltd, Singapore.
454 Mota, R., Monteiro Santos, F. A., Mateus, A., Marques, F. O., Gonçalves, M. A., Figueiras,
455 J., et al. (2004). Granite fracturing and incipient pollution beneath a recent landfill
456 facility as detected by geoelectrical surveys. Journal of Applied Geophysics, 57(1), 11-
457 22, doi:http://dx.doi.org/10.1016/j.jappgeo.2004.08.007.
458 NJDEP (2005). Field sampling procedures manual. (Vol. Chapter 8, pp. 1-46). New Jersey.
459 Peace, J. L., Hyndman, D. A., & Goering, T. J. (1996). Application of Non-intrusive
460 Geophysical Techniques at the Mixed Waste Landfill, Technical Area 3, Sandia
461 National Laboratories, New Mexico: Sandia National Laboratories.
462 Pridmore, D. F., Hohmann, G. W., Ward, S. H., & Sill, W. R. (1981). An investigation of
463 finite-element modeling for electrical and electromagnetic data in three dimensions.
464 Geophysics, 46(7), 1009-1024, doi:doi:10.1190/1.1441239.
465 Rattanaoudom, R. (2005). INVESTIGATION ON TOXICITY AND HAZARDOUS NATURE
466 OF A MUNICIPAL SOLID WASTE DUMPSITE. Asian Institute of Technology,
467 Thailand.
468 Reynolds, J. M., & Taylor, D. I. (1996). Use of geophysical surveys during the planning,
469 construction and remediation of landfills (Vol. 11, Engineering geology of waste
470 disposal). London: The Geological Society of London.
471 Rosqvist, H., & Destouni, G. (2000). Solute transport through preferential pathways in
472 municipal solid waste. Journal of Contaminant Hydrology, 46(1–2), 39-60,
473 doi:http://dx.doi.org/10.1016/S0169-7722(00)00127-3.

474 Samouëlian, A., Richard, G., Cousin, I., Guérin, R., Bruand, A., & Tabbagh, A. (2004).
475 Three-dimensional crack monitoring by electrical resistivity measurement. European
476 Journal of Soil Science, 55(4), 751-762, doi:10.1111/j.1365-2389.2004.00632.x.
477 Sandberg, S. K., Slater, L. D., & Versteeg, R. (2002). An integrated geophysical investigation
478 of the hydrogeology of an anisotropic unconfined aquifer. Journal of Hydrology,
479 267(3–4), 227-243, doi:http://dx.doi.org/10.1016/S0022-1694(02)00153-1.
480 Simões, G. F., & Catapreta, C. A. A. (2013). Monitoring and modeling of long-term
481 settlements of an experimental landfill in Brazil. Waste Management, 33(2), 420-430,
482 doi:http://dx.doi.org/10.1016/j.wasman.2012.10.001.
483 Soupios, P., Papadopoulos, N., Papadopoulos, I., Kouli, M., Vallianatos, F., Sarris, A., et al.
484 (2007). Application of integrated methods in mapping waste disposal areas.
485 Environmental Geology, 53(3), 661-675, doi:10.1007/s00254-007-0681-2.
486 Svensson, M., Bernstone, C., & Dahlin, T. (1999). The Combination of the SASW Method
487 and DC-Resistivity in Characterization of Old Landfills. In Symposium on the
488 Application of Geophysics to Engineering and Environmental Problems 1999 (pp. 123-
489 131).
490 Tame, C., Cundy, A. B., Royse, K. R., Smith, M., & Moles, N. R. (2013). Three-dimensional
491 geological modelling of anthropogenic deposits at small urban sites: A case study from
492 Sheepcote Valley, Brighton, UK. Journal of Environmental Management, 129(0), 628-
493 634, doi:http://dx.doi.org/10.1016/j.jenvman.2013.08.030.
494 Wall, D., & Zeiss, C. (1995). Municipal Landfill Biodegradation and Settlement. Journal of
495 Environmental Engineering, 121(3), 214-224, doi:doi:10.1061/(ASCE)0733-
496 9372(1995)121:3(214).

497 Wightman, W. E., Jalinoos, F., Sirles, P., & Hanna, K. (2003). Application of Geophysical
498 Methods to Highway Related Problems. Lakewood, CO: Federal Highway
499 Administration.
500 Wu, B.-J., Zhu, Z.-D., & Gu, Z.-J. (2013). Study on Accuracy of Soil Slope Stability
501 Analysis Based on Strength Reduction FEM. Journal of Water Resources and
502 Architectural Engineering, 11(1), 17-21.
503 Yin, K., Tong, H. H., Noh, O., Wang, J.-Y., & Giannis, A. (2015). Mapping Refuse Profile in
504 Singapore Old Dumping Ground through Electrical Resistivity, S-Wave Velocity and
505 Geotechnical Monitoring. Bulletin of Environmental Contamination and Toxicology,
506 94(3), 275-281, doi:10.1007/s00128-014-1427-y.
507 Zekkos, D., Sahadewa, A., Woods, R. D., & II, K. H. S. (2014). Development of Model for
508 Shear-Wave Velocity of Municipal Solid Waste. Journal of Geotechnical and
509 Geoenvironmental Engineering, 140(3), 04013030, doi:doi:10.1061/(ASCE)GT.1943-
510 5606.0001017.
511

512 Table and Figures

513 Table 1.Geotechnical analysis of soil samples from borehole BH1-5 at depth of 3-7 m.

Borehole No.		BH1			BH2			BH3			BH4		BH5		
Depth		3-3.7	4.5-5.2	6-6.9	3-4.2	4.5-5.2	6-6.8	3-3.5	4.5-5.3	6-6.6	3-3.5	6-6.25	3-3.5	4.5-5.4	6-6.8
Water%		14	30	25	22	24	31	19	23	17	20	24	39	38	35
Bulk density (g/cm^3)		1.79	1.93	1.81	1.98	1.93	1.79	2.01	1.99	2.00	2.06	1.76	1.83	1.87	1.93
Dry density (g/cm^3)		1.57	1.48	1.45	1.62	1.56	1.37	1.69	1.62	1.71	1.72	1.42	1.32	1.46	1.43
Particle density (g/cm^3)		2.65	2.71	2.70	2.70	2.72	2.70	2.67	2.71	2.66	2.71	2.60	2.67	2.68	2.69
Void%		40.8	45.4	46.3	40.0	42.6	49.3	36.7	40.2	35.7	36.5	45.4	50.6	45.5	46.8
Particle size%	Gravel	11	14	6	N.A.	10	6	6	5	14	3	22	15	7	14
	Sand	77	46	57	N.A.	54	42	60	29	59	32	52	66	60	50
	Silt	11	28	28	N.A.	22	38	15	34	11	41	19	17	14	16
	Clay	1	12	9	N.A.	14	14	19	32	16	24	7	2	19	20
Chemical test	OM%	N.A.	N.A.	2.1	1.5	N.A.	N.A.	0.5	N.A.	N.A.	0.1	1	N.A.	2.9	1.8
	S%	N.A.	N.A.	<0.01	<0.01	N.A.	N.A.	<0.01	N.A.	N.A.	<0.01	<0.01	N.A.	<0.01	0.15
	Cl^-%	N.A.	N.A.	0.06	<0.01	N.A.	N.A.	0.04	N.A.	N.A.	0.03	0.05	N.A.	0.23	0.19
	pH	N.A.	N.A.	9.3	7.7	N.A.	N.A.	8.7	N.A.	N.A.	9.2	8	N.A.	8.9	9.7
Atter-berg Limit	Liquid limit	N.A.	37	49	40	40	40	40	47	26	38	41	51	37	38
	Plasticity limit	N.A.	28	31	27	29	28	16	30	12	26	29	30	16	15
	Plasticity Index	N.A.	9	18	13	11	12	24	17	14	12	12	21	21	23
	Soil group	N.A.	MI	MI	MI	MI	MI	CL	MI	CL	MI	MI	MH	CL	CL

514

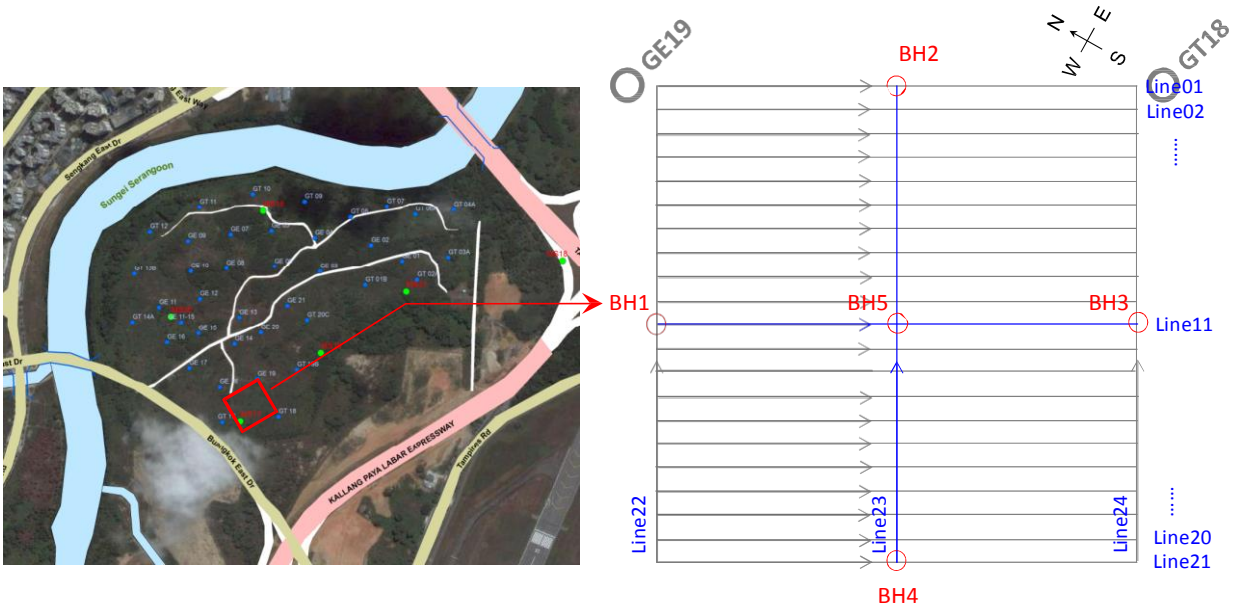

Figure 1. Site map and borehole locations indicated by the geophysical layout at LHDG.p3.

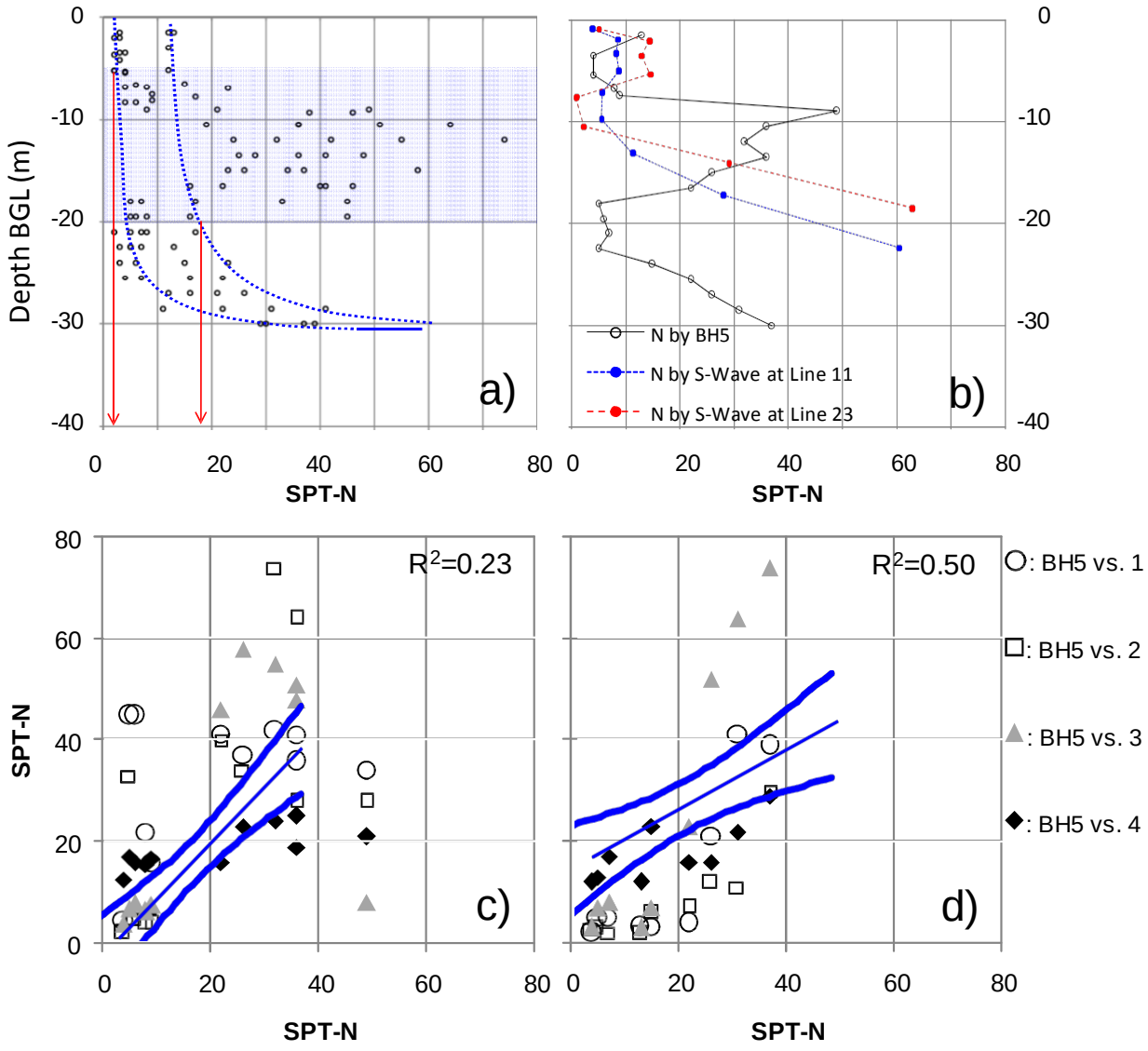

Figure 2a) Standard penetration test n (SPT-N) value plotting from the borehole (BH1-5) investigation at LHDG.p3; 2b) SPT-N value at BH5 vs. estimation based on S-Wave velocity using eq. 1 at Line 11 and 23, respectively; 2c) SPT-N values between BH5 vs. BH1-4 respectively at depth 5-20 m below ground level (BGL); 2d) SPT-N values between BH5 vs. BH1-4 respectively at depth 0-5 m & 20-30 m BGL (Note: curved lines in Fig. 2b-c represent the 95% confidence interval of the least squares linear regressions).

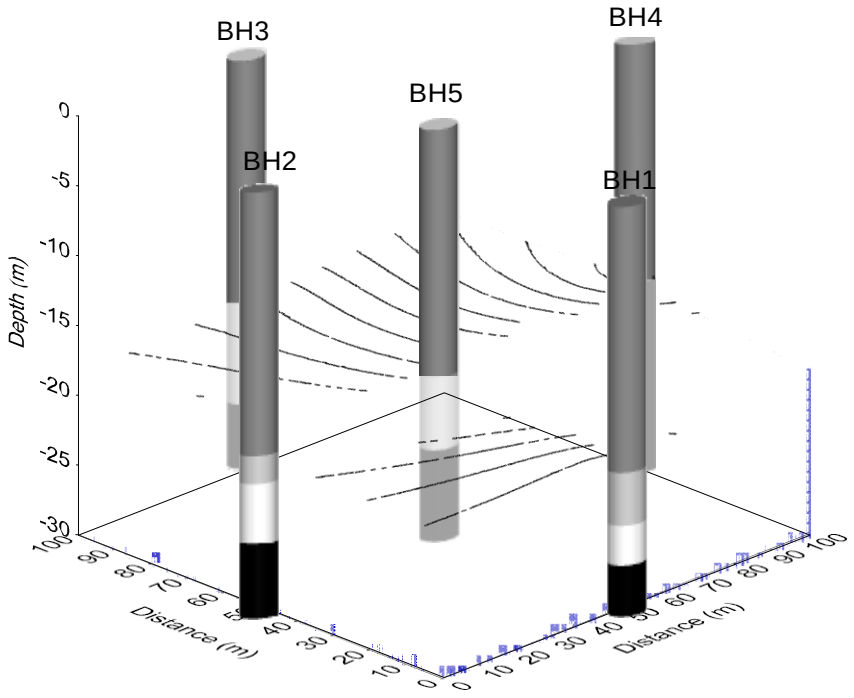

525

526 Figure 3. Estimation of refuse boundary with bore logs (BH1-5) in 2013.

527

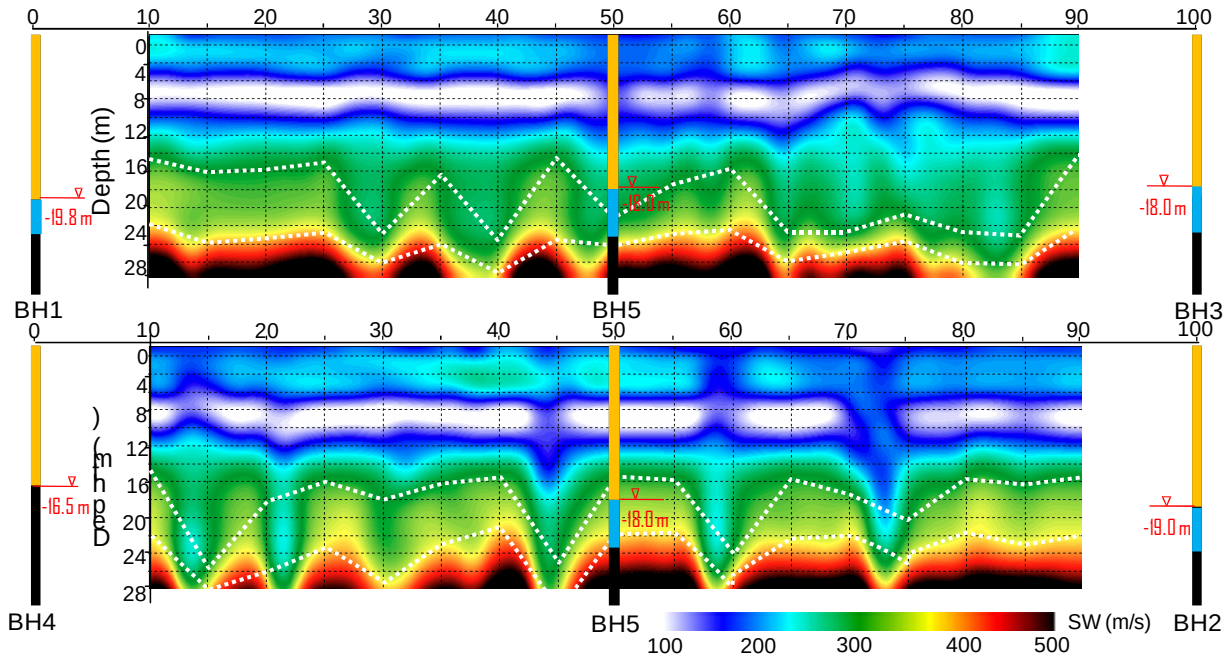

528

Figure 4. Boundary estimation by the pseudo 2D image of surface wave velocity (at line 11 & 23) and by BH1-5-3 and BH2-5-4, respectively.

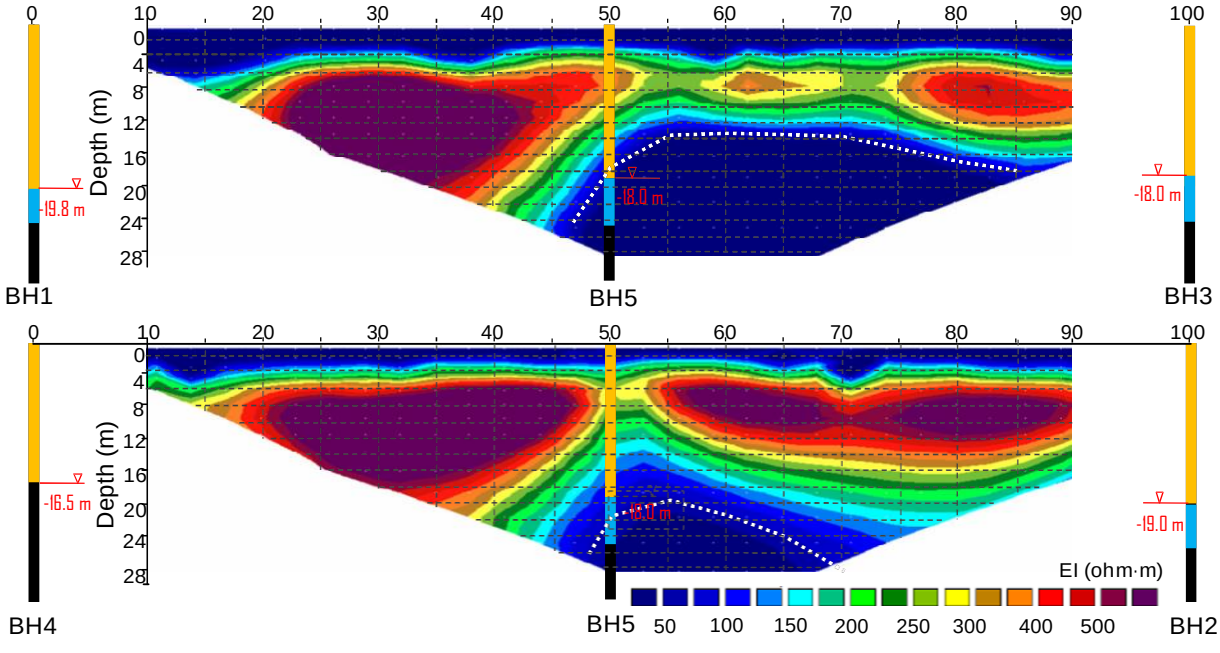

Figure 5. Boundary estimation by the 2D resistivity (at line 11 & 23) and by BH1-5-3 and BH2-5-4, respectively.

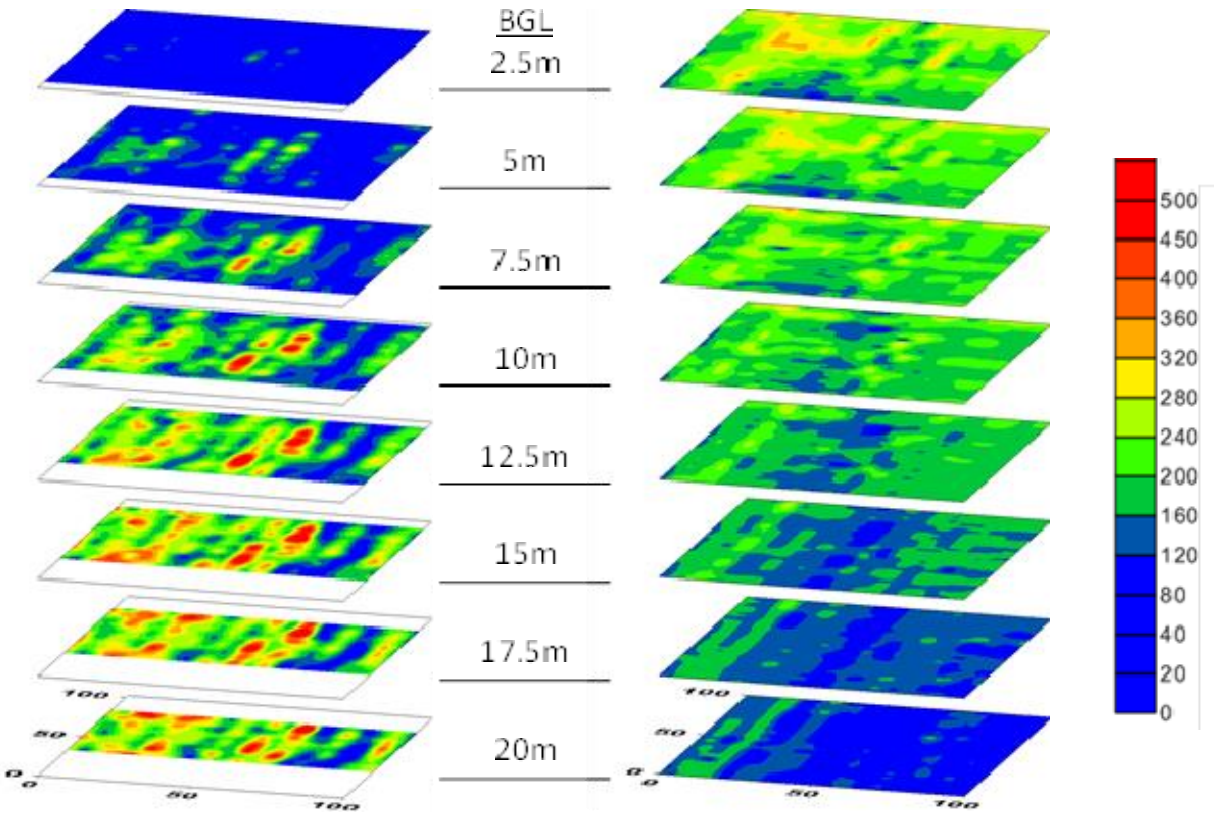

Figure 6. Comparison of EI pseudo-depth slices between 2013 (Left) and 2011(Right).

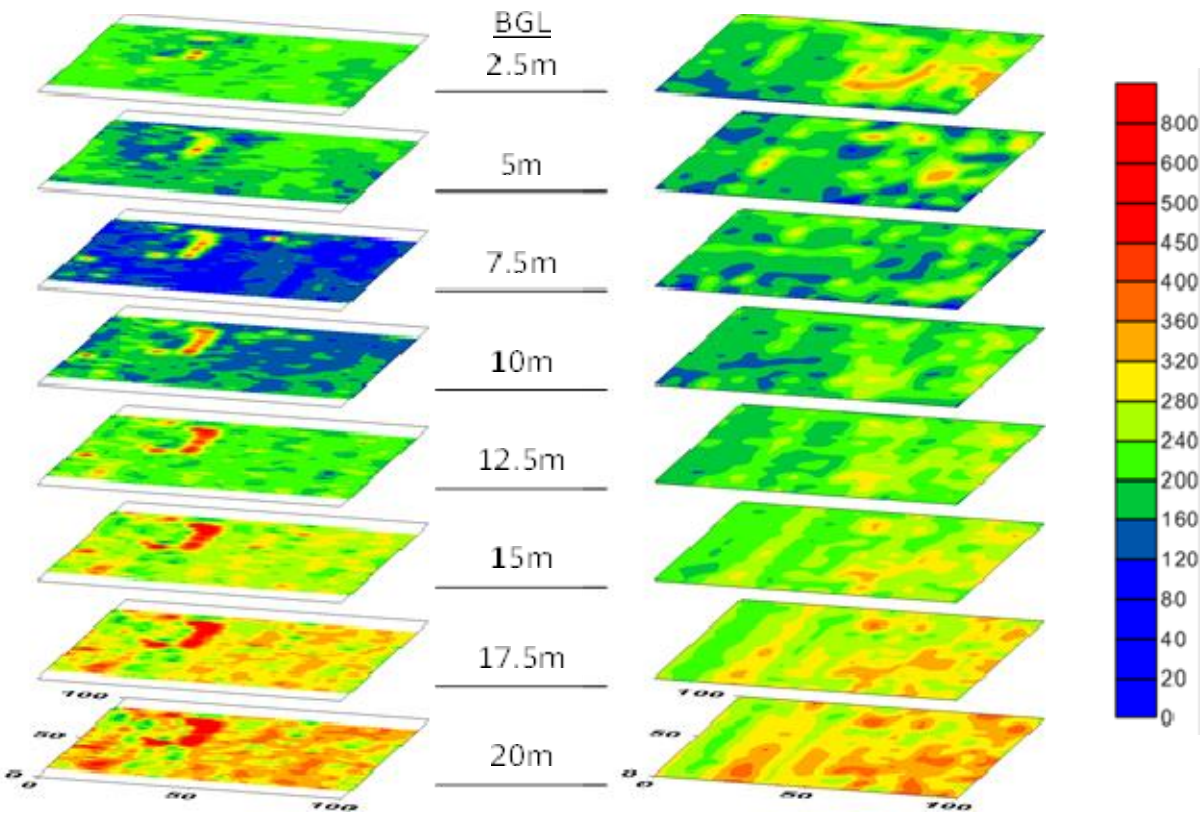

538

539 Figure 7. Comparison of MASW pseudo-depth slices between 2013 (Left) and 2011(Right).

540

Supplementary material

Table S1. Statistical correlations between geophysical values (S-wave velocity and ER) and soil characters at soil sample locations (BH1-5).

F

Parameters		Correlation coefficient	
		S-wave (m/s)	ER (Ω m)
Water%		-0.11	0.66
Bulk density (g/cm^3)		0.36	-0.09
Dry density (g/cm^3)		0.35	-0.40
Particle density (g/cm^3)		0.20	0.03
Void%		-0.33	0.41
Particle size%	Gravel	-0.37	0.03
	Sand	0.09	0.06
	Silt	-0.13	-0.26
	Clay	0.25	0.21
Chemical test	OM%	-0.20	0.61
	S%	N.A.	N.A.
	Cl^-%	0.13	0.93
	pH	-0.25	0.64
Atter-berg Limit	Liquid limit	0.17	-0.09
	Plasticity limit	-0.05	-0.52
	Plasticity Index	0.28	0.60
	Soil group	N.A.	-0.09

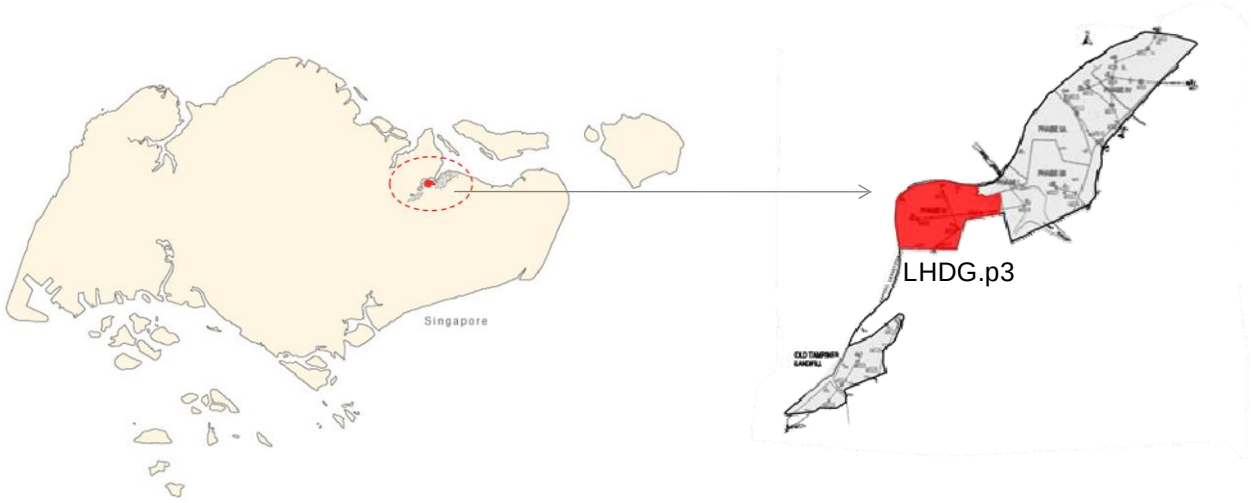

Figure S1. Studied site (LHDG.p3) at Lorong Hulas dumping ground in Singapore.

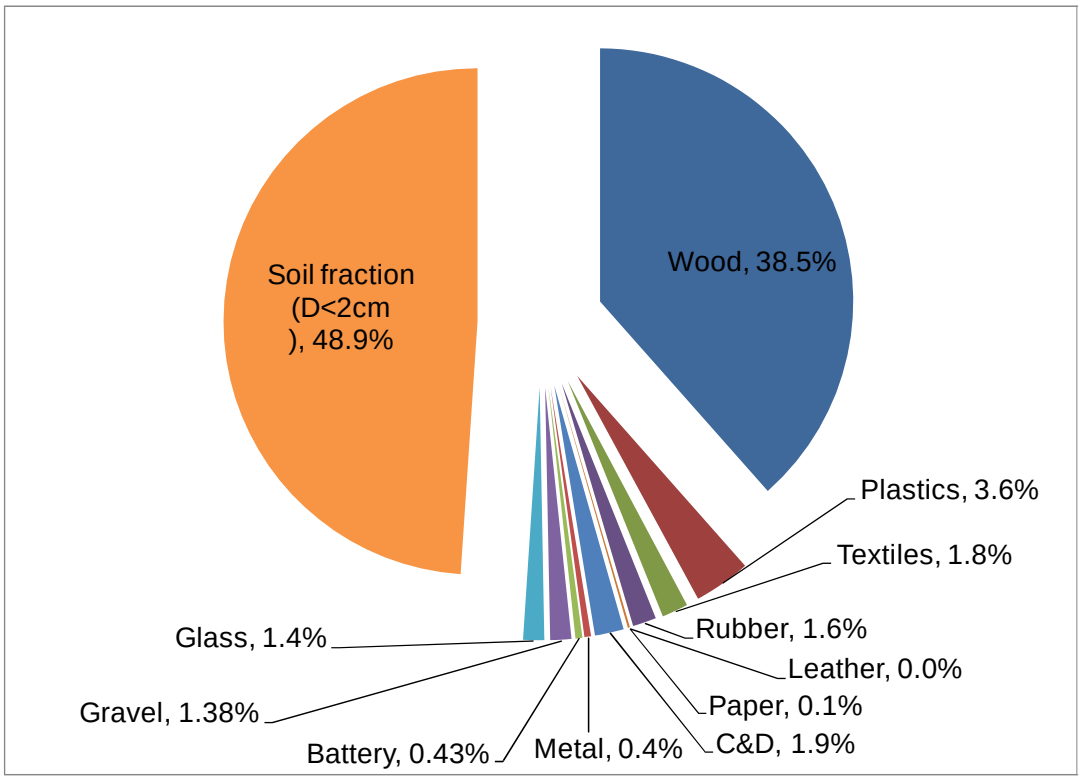

549

550 Figure S2. Refuse composition analysis at depth -8-15m in the plot in 2013.

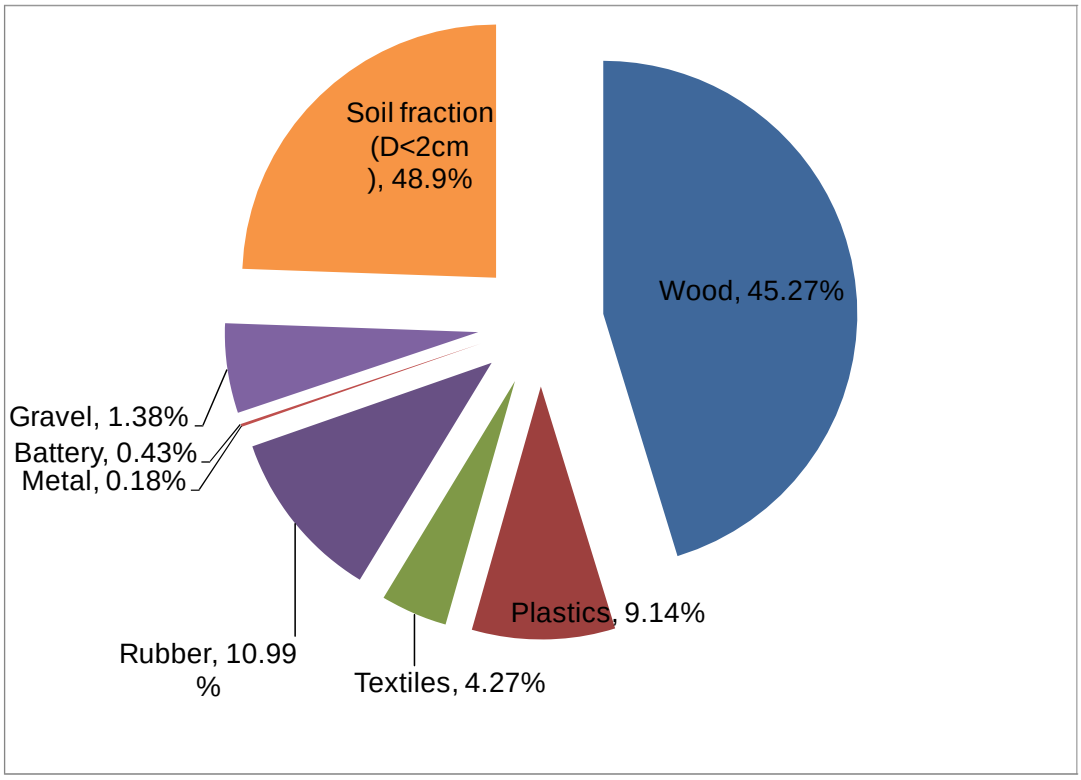

551

552 Figure S3. Refuse composition analysis at depth -8-10m in the plot in 2013.